frontiers | Frontiers in Astronomy and Space Sciences

TYPE Original Research
PUBLISHED 02 October 2023
DOI 10.3389/fspas.2023.1199711

OPEN ACCESS

EDITED BY
Gian Luca Delzanno,
Los Alamos National Laboratory (DOE), United States

REVIEWED BY
Andris Vaivads,
Ventspils University College, Latvia
Takayuki Umeda,
Nagoya University, Japan

*CORRESPONDENCE
Katherine Goodrich,
katherine.goodrich@mail.wvu.edu

RECEIVED 03 April 2023
ACCEPTED 04 September 2023
PUBLISHED 02 October 2023

CITATION
Goodrich K, Cohen IJ, Schwartz S, Wilson LB III, Turner D, Caspi A, Smith K, Rose R, Whittlesey P and Plaschke F (2023), The multi-point assessment of the kinematics of shocks (MAKOS). *Front. Astron. Space Sci.* 10:1199711. doi: 10.3389/fspas.2023.1199711

The multi-point assessment of the kinematics of shocks (MAKOS)

Katherine Goodrich[1]*, Ian J. Cohen[2], Steven Schwartz[3,4], Lynn B. Wilson III[5], Drew Turner[2], Amir Caspi[6], Keith Smith[7], Randall Rose[6], Phyllis Whittlesey[8] and Ferdinand Plaschke[9]

[1]Department of Physics and Astronomy, West Virginia University, Morgantown, WV, United States, [2]Applied Physics Laboratory, John Hopkins University, Laurel, MD, United States, [3]Laboratory for Atmospheric and Space Physics, University of Colorado, Boulder, CO, United States, [4]Imperial College London, London, United Kingdom, [5]Goddard Space Flight Center, Laurel, MD, United States, [6]Southwest Research Institute, Boulder, CO, United States, [7]Southwest Research Institute, San Antonio, TX, United States, [8]Space Sciences Laboratory, University of California, Berkeley, CA, United States, [9]Technische Universität Braunschweig, Branschweig, Germany

Collisionless shock waves are one of the main mechanisms of energy conversion in space plasmas. They can directly or indirectly drive other universal plasma processes such as magnetic reconnection, turbulence, particle acceleration and wave phenomena. Collisionless shocks employ a myriad of kinetic plasma mechanisms to convert the kinetic energy of supersonic flows in space to other forms of energy (e.g., thermal plasma, energetic particles, or electromagnetic energy) in order for the flow to pass an immovable obstacle. The partitioning of energy downstream of collisionless shocks is not well understood, nor are the processes which perform energy conversion. While we, as the heliophysics community, have collected an abundance of observations of the terrestrial bow shock, instrument and mission-level limitations have made it impossible to quantify this partition, to establish the physics within the shock layer responsible for it, and to understand its dependence on upstream conditions. This paper stresses the need for the first ever spacecraft mission specifically designed and dedicated to the observation of both the terrestrial bow shock as well as Interplanetary shocks in the solar wind. Our mission concept, the Multi-point Assessment of the Kinematics of Shocks (MAKOS), will greatly improve on previous observations of the terrestrial bow shock with instrumentation specifically tailored to observe the evolution of the solar wind through the shock.

KEYWORDS

collisionless shock, bow shock, wave-particle interaction, mission concept study, space plasma instrumentation

1 Science description

1.1 MAKOS science questions

Understanding collisionless shocks is vital to the understanding of our Universe, from the heating and deflection of bulk flows to the acceleration of cosmic rays. Moreover, collisionless shocks directly influence our own terrestrial space environment, e.g., solar wind-magnetosphere interactions.

Vital questions regarding collisionless shocks remain unanswered:

1. What is the partition of energy across collisionless shocks?
2. What are the processes governing energy conversion at and within collisionless shocks?
3. How and why do these processes vary with macroscopic shock parameters?

In this paper, we will discuss why addressing these questions is of critical importance. The path forward to make significant progress towards addressing these questions is through the implementation of MAKOS (Multi-point Assessment of the Kinematics of Shocks) an STP class mission consisting of four satellites with a full particle and fields instrument suite. This paper will also describe the concept of the MAKOS mission. This includes a description of its payload, concept of operations, and the technological enhancements needed to implement MAKOS to its greatest effect.

1.2 Background and motivation

Shocks are spatial discontinuities that form when a supersonic flow encounters an obstacle. If the medium travels faster than the speed of communication, the medium has no time to smoothly adjust its trajectory. A shock forms ahead of the obstacle and slows the supersonic flow to subsonic speeds in order for the medium to travel past. In high density media, the shock structure and evolution are governed by particle collisions. In space, however, the majority of shocks are collisionless, making the dominant mechanisms of energy conversion difficult to define.

The most relevant collisionless shock to humans, and the one most often measured *in situ*, is the terrestrial bow shock. The terrestrial bow shock is also significantly more straightforward to observe relative to Interplanetary (IP) shocks in the solar wind, as it remains in the same spatial position relative to Earth (to within a few Earth rad ii). Therefore, we derive the majority of our knowledge of collisionless shock dynamics from the terrestrial bow shock.

The solar wind inputs primarily bulk proton ram energy upstream of the bow shock. However, the shock outputs energy in several different forms. These include, but are not limited to, electron, proton and heavy ion acceleration and heating, together with Poynting flux and turbulent fluctuations. Previous missions together with numerical simulations have provided invaluable insight to the overall structure and behavior of the terrestrial bow shock [e.g. (Burgess, 2015)]. Past missions that have observed the terrestrial bow shock include MMS, THEMIS, Cluster, Wind, AMPTE, and ISEE. They have confirmed that the shock can exist as a nonstationary discontinuity. It can act as a "breathing barrier" between the solar wind and the terrestrial magnetosphere, changing in response to varying upstream conditions.The spatial scale, energy conversion processes, and output of the shock are most heavily dependent on the orientation of the Interplanetary Magnetic Field (IMF) relative to the shock normal vector ($\hat{n}$) and the fast magnetosonic Mach number (M_f). Shocks are generally categorized as either Quasi-perpendicular ($Q_\perp$) or Quasi-parallel ($Q_\parallel$) depending on whether the angle between the IMF and shock normal (θ_{Bn}) is greater than or less than 45°. The terrestrial bow shock also tends to grow more turbulent in nature as the Mach number (M_f) increases and as the plasma β decreases.

Figure 1 summarizes the complexity of the global structure of the terrestrial bow shock. At $Q_\perp$ shocks (i.e., toward the top of the figure), particle motion in the shock-normal direction is restricted by the Lorentz force to within one gyroradius in the upstream direction. Thus, $Q_\perp$ shocks tend to have short coherent transition regions, with quasi-static magnetic and electric fields making the largest contributions to the bulk particle dynamics.

$Q_\parallel$ shocks (bottom of Figure 1) permit particle traversals in both directions across the shock, including well into the upstream region. Such shocks exhibit an extended transition region and are dominated by strongly varying particle sub-populations, particle reflection with corresponding kinetic instabilities and turbulence, and particle acceleration. They can also be populated with foreshock transient events such as hot flow anomalies (Schwartz et al., 2018) and foreshock bubbles (Turner et al., 2013), which can locally generate their own shocks and foreshocks (Wilson et al., 2013; Wilson et al., 2016) in poorly understood ways.

1.3 Necessary measurements for science closure

While it is known that collisionless shocks perform energy conversion, specifically to process the bulk flow kinetic energy density (Wilson et al., 2014a; Wilson et al., 2014b; Chen et al., 2018; Goodrich et al., 2018), the details of this energy conversion and output remain unclear. The kinetic-scale processes that perform this energy conversion are not well known or well observed within the terrestrial bow shock. Moreover, it is not clear what the resulting energy budget is once the plasma traverses the shock or how it varies for different shock conditions. In this section, we describe the scientific motivation of MAKOS science questions and the measurements necessary to address them.

1.3.1 What is the partition of energy across collisionless shocks?

In order to understand how energy is partitioned in the shock, it is important to accurately resolve the types and weights of different energy inputs and outputs of the system. Simultaneously relating upstream and downstream conditions remains a persistent challenge in studying shock physics as it necessitates simultaneous, complementary, and inter-calibrated upstream and downstream measurements of the plasma.

Important energy fluxes include those related to particle bulk flow, thermal and energetic/nonthermal energy for multiple, relevant species (protons, alphas, heavy ions, and electrons), together with electromagnetic energy. The different energies related to particle species require measurements of full velocity distribution functions. The thermal properties, anisotropies, and non-Maxwellian thermal features of the cool incident solar wind populations (i.e., electrons, protons, and alphas <1 keV) as well as higher energy particles (i.e., electrons, H, He, C, N, O, Ne, and Fe > 1 keV) must also be resolved. Crucially, the cold thermal solar wind plasma beam must be fully resolved without compromising the measurement of the hot, shocked plasma or suprathermal reflected and accelerated particles.

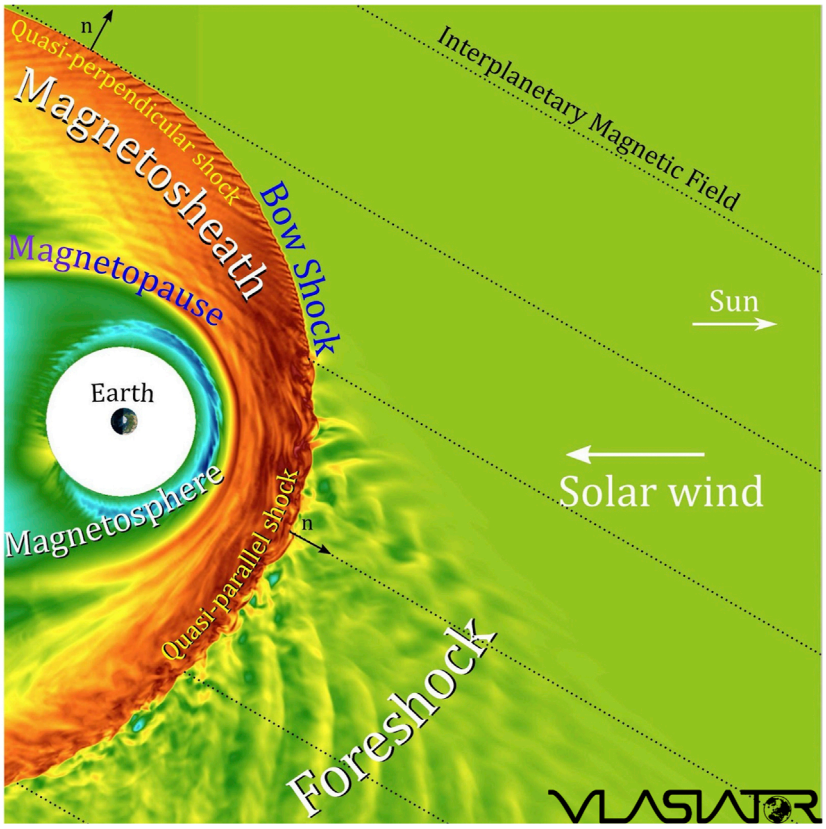

FIGURE 1
Schematic of the terrestrial bow shock, taken from European Commission (2021). Color shading indicates electromagnetic wave activity. Note the extended turbulent structure at the quasi-parallel shock (toward the bottom) by comparison to that at the quasi-perpendicular shock (toward the top).

The majority of the upstream energy flux consists of proton ram energy flux while proton enthalpy flux comprises the majority of the downstream partition (Schwartz et al., 2022), as seen in Figure 2. The shock can also produce other significant energy fluxes including that in accelerated particles, nonthermal features and DC/AC Poynting flux or turbulence. Although these energy fluxes are considered minor contributions to the energy partition, they can be significant to the overall dynamics of the shock, or to the nature of the interaction of the shocked plasma with the magnetosphere.

Two crucial factors must be considered here. Firstly, the upstream and downstream plasma must be observed in correlation in order to ensure that the output energy fluxes are matched to the measured inputs. Secondly, the upstream plasma must be measured in such a way that it is clearly not perturbed by conditions of the shock itself, i.e., reflected particles, ultra-low frequency waves, and foreshock phenomena.

Historically, magnetospheric missions have lacked one or more capabilities to solve this problem. Those capabilities include matched up/downstream measurements, comprehensive inter-calibrated instrumentation, time resolution, velocity-space resolution, and spacecraft separations. According to Schwartz et al. (2022), progress can be made with observations from MMS (as shown in Figure 2), in which it was found that normal energy flux is conserved to within 3%. However, this requires significant assumptions. The most critical of which are the solar wind parameters must be acquired from Wind and the mass requires manual adjustments to remain conserved. This confirms that even advaned missions like MMS cannot provide sufficient observations to resolve the energy partition across shocks. These results are fully detailed in Schwartz et al. (2022).

Without a full account of the energy partition, our modeling and simulation knowledge of shocks, and the applicability of that knowledge to more distant space environments, is at a significant disadvantage. Improvements can and must be made to allow for these observations. MAKOS will do this by engaging four spacecraft with varied spacing (see Figure 8). Two of the four spacecraft (separated at ion kinetic scales, ~1,000 km) will act as upstream monitors with apogees up to 25 Earth radii. The two remaining spacecraft (spaced ~100 s km apart) will be separated from the upstream monitors by several Earth radii anti-sunward in order observe the resulting magnetosheath.

1.3.2 What are the processes governing energy conversion at and within collisionless shocks?

The knowledge of several different conversion mechanisms have been listed. These include, but are not limited to, a cross-shock electrostatic potential (Tsurutani and Rodriguez, 1981; Chen et al., 2018), current-driven instabilities such as the Buneman (Bale and Mozer, 2007; Goodrich et al., 2018) and electron-cyclotron drift instability (Breneman et al., 2013), magnetic reconnection

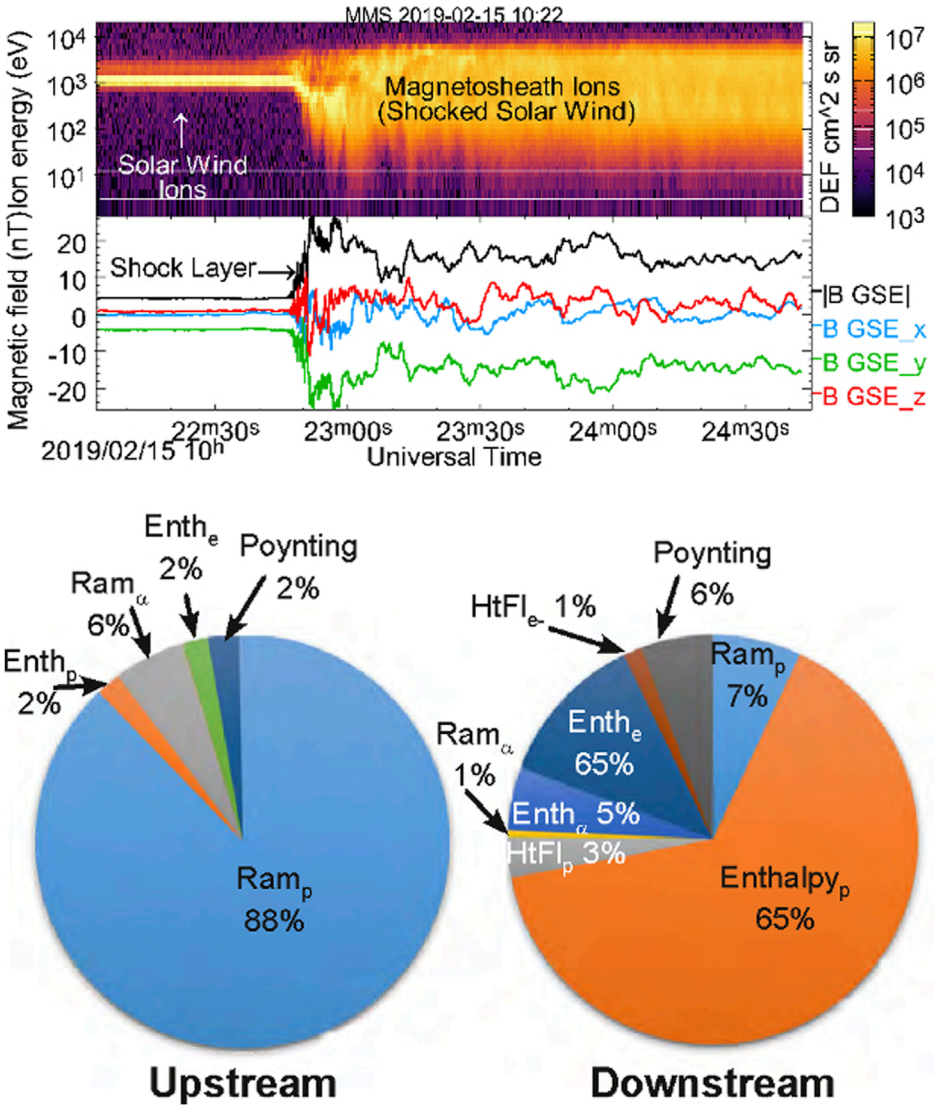

FIGURE 2
Documented energy partition upstream and downstream of an example shock crossing [taken from Schwartz et al. (2022)]. The upstream energy flux is dominated by the proton bulk flow ram energy. It gets partitioned across the particle populations downstream. The relative proportions depend on the upstream parameters in unknown ways.

(Wang et al., 2016; Gingell et al., 2017), and other wave-particle interactions (Chen et al., 2018; Vasko et al., 2018; Goodrich et al., 2019), and particle acceleration and reflection. We know, for example, that at even modest Mach number $Q_\perp$ shocks, particle reflection initiates the dispersal in velocity space that results in a higher second moment (temperature). The balance between that mechanism and others within the shock layer that act on both the incident protons and other species is not understood. It is also unknown how these mechanisms change with upstream conditions, or if the presence of one mechanism drastically alters the resultant downstream plasma.

Within the shock, energy is converted on the kinetic scale (see above references). This inherently renders MHD modeling insufficient to accurately simulate collisionless shocks in their full complexity. We have learned much from PIC and Vlasov simulations, but we have yet to provide observational confirmation. Historically, *in-situ* spacecraft have relied on particle detectors that can resolve full velocity distribution functions (VDFs) over one full spin period, on the order from one to tens of seconds. Observed bow shock crossings can have observational lifetimes on the order of seconds, rendering past particle resolution insufficient.

MMS shock observations, with high-temporal resolution, allow us to correlate wave and particle behavior like never before. Figure 3, taken from Goodrich et al. (2019) show bursty ion acoustic-like waves are seen in correlation with impulsive reflected ion populations. This study showed electrostatic waves can correspond to short time-scale particle activity within collisionless shocks. Despite its capabilities, however, MMS has significant limitations in its capability to observe shock phenomena. We describe these limitations in detail within the following section.

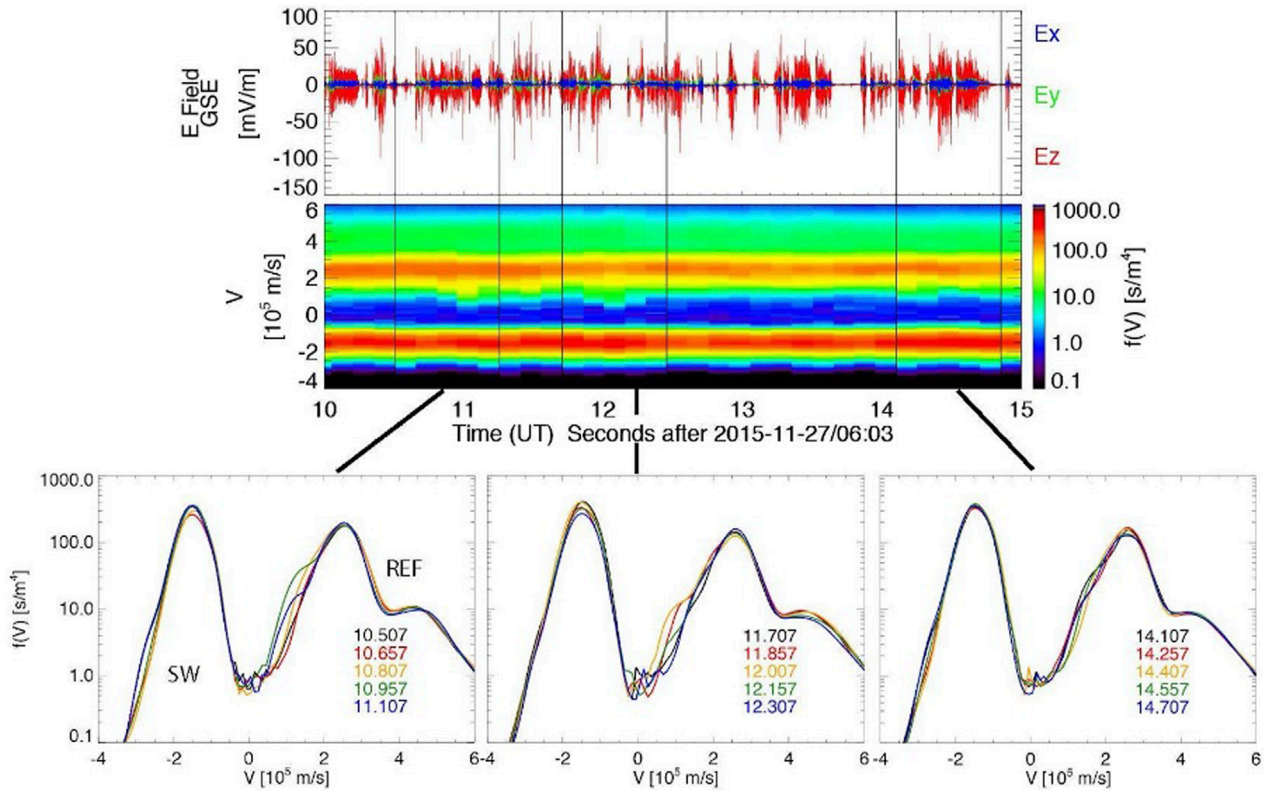

FIGURE 3
Comparison of 2D ion velocity distributions and electrostatic waves. Bursty electric fields (top) can be linked to fast time variations in particle reflection off the shock which manifests itself in fine scale structure in velocity. This illustrates the interplay between the macroscopic shock inputs and the processes responsible for ultimately converting that energy to other forms. (Taken from Goodrich et al. (2019)).

To bring closure to this question, we must measure full velocity distribution functions at a high time resolution (10s of ms for electrons) with an energy and angular resolution specified for the solar wind ion distribution. The proposed MAKOS mission intends to develop and outfit such particle instruments. In addition to the DC fields that govern the lowest order particle dynamics, MAKOS will also measure high frequency electric and magnetic field oscillations to identify local plasma instabilities and estimate the amount of energy carried away from the shock region by plasma waves. Using these measurements, plasma instabilities and energy conversion mechanisms will be quantified and distinguished within the shock and then correlated with the energy budgets measured by the spacecraft situated upstream and downstream of the shock.

1.3.3 How and why do these processes vary with macroscopic shock parameters?

The final question is how the energy partitioning process and outputs are related to the shock's driving conditions. It is known that θ_{Bn} can influence the geometry and size of the shock, as well as its deviation from laminar behavior. It is not known, however, how θ_{Bn} can influence the energy budget or energy conversion processes that may occur. The same can be said of the upstream fast magnetosonic Mach number (M_f) and plasma beta (β), the presence of He^2+ and/or other minor ion populations, thermal anisotropies, temperatures of both electrons and the various ion species, and the contributions of energetic particle populations.

The employment of MAKOS will answer this question by observing a statistically significant number of shock crossings with a range of driving conditions, quantifying parametric dependencies of various energy partitioning configurations and energy conversion processes vs. shock orientations and driving conditions. The dataset that will result from MAKOS will provide measurements of >500 quasiparallel and quasi-perpendicular shocks each, assuming they are each observed with approximately equal probability. This will provide sufficient statistics to identify trends in the energy budget and identified energy conversion processes due to specific shock input conditions. Furthermore, the MAKOS orbits offer year-round coverage in the solar wind, also enabling MAKOS to study interplanetary shocks and further bolster the statistics on various shock driving conditions and behavior.

1.4 Science Traceability Matrix

Figure 4 shows an abridged version of the MAKOS Science Traceability Matrix with the mapping to the science questions listed above. The MAKOS mission design, instrumentation suite, cost/risk analysis, and enhancing technological developments are summarized in "Investigation Description".

MAKOS Science Traceability Matrix

Science Questions	Science Objectives	Physical Parameters	Observable Quantities	Instrument
[Q1] What is the energy budget both upstream and downstream of a collisionless shock?	Quantify the contribution of proton and electron thermal and kinetic energy to the shock energy budget	Simultaneous upstream and downstream moments (density, velocity, pressure, heat flux) of particle sub-populations	Simultaneous upstream and downstream core 3D velocity distribution functions	SWI
				SWE
			Simultaneous upstream and downstream suprathermal 3D velocity distribution functions	STI
	Quantify the contribution of He and the CNO group thermal and kinetic energy to the shock energy budget			STE
			Simultaneous upstream and downstream energetic particle energy, angular, and compositional distributions	EP
	Quantify the contribution of Poynting flux to the shock energy budget	Electric and Magnetic field contribution to the Poynting flux	Simultaneous upstream and downstream 3D DC- and AC-coupled electric and magnetic field	EFI
				FGM
				SCM
[Q2] What are the processes governing energy conversion at and within collisionless shocks?	Characterize the coherent and incoherent heating and acceleration of particle populations upstream, downstream, and within the shock front	Particle heating	Simultaneous upstream, within shock, and downstream core, suprathermal and energetic particle 3D Velocity Distribution Functions (VDFs)	SWI
				SWE
				STI
				STE
				EP
	Identify electric and magnetic field variations together with targeted local plasma instabilities and resulting waves within the shock	Non-Maxwellian features responsible for observed instabilities	Simultaneous upstream, within shock, and downstream core 3D VDFs	SWI
				SWE
			Simultaneous upstream, within shock, and downstream suprathermal 3D VDFs	STI
				STE
		Magnetic and electric field topology and wave modes	Simultaneous upstream, within shock, and downstream 3D DC- and AC-coupled magnetic and electric field	FGM
				SCM
				EFI
[Q3] How and why do these processes vary with shock orientation and driving conditions?	Parameterize shock crossings according to the macroscopic, Rankine-Hugoniot relations	Particle-dependent macroscopic shock parameters.	Upstream, within shock, and downstream particle moments and 3D DC-coupled magnetic field	All
	Tabulate and sort observed shock crossings according to the macroscopic shock parameters for statistical analysis of science objectives	Statistical parameterization of the processes in [Q1] & [Q2] versus calculated shock parameters		All

Instrument Requirements			
Instrument & Parameter		Measurement Req.	Exp. Data Volume per Orbit
SWI	Energy Range	300 eV – 7 keV	27 GB
	Energy Resolution	10%	
	FOV	40° x 40°	
	Angular Resolution	6°	
	Temporal Resolution	0.1 s	
SWE	Energy Range	3 eV – 1.5 keV	314 GB
	Energy Resolution	10%	
	Angular Coverage	4π-ster	
	Angular Resolution	20°	
	Temporal Resolution	0.01 s	
STI	Energy Range	700 eV – 30 keV	102 GB
	Energy Resolution	20%	
	Angular Coverage	4π-ster	
	Angular Resolution	20°	
	Temporal Resolution	1 s	
STE	Energy Range	500 eV – 30 keV	13 GB
	Energy Resolution	20%	
	Angular Coverage	4π-ster	
	Angular Resolution	20°	
	Temporal Resolution	1 s	
EP	Energy Range	20 keV– 10 MeV	30 GB
	Energy Resolution	20%	
	Species	H, He, C, O, Ne, e⁻	
	FOV	180°	
	Angular Resolution	30°	
	Temporal Resolution	1 s	
FGM	(DC) Dynamic Range	±500 nT	278 MB
	Resolution	10 pT	
	Temporal Resolution	0.03125 s	
SCM	(AC) Dynamic Range	±50 nT	12 GB
	Resolution	0.1 pT	
	Temporal Resolution	0.001 s	
EFI	(DC) Range	±1000 mV/m	115 GB
	Dimensions	3	
	Resolution	1 mV/m	
	Temporal Resolution	0.5 s	
	(AC) Range	±2000 mV/m	
	Dimensions	3	
	Resolution	1 mV/m	
	Temporal Resolution	0.001 s	

FIGURE 4
MAKOS will address outstanding questions regarding the cross-scale physical processes at play at collisionless shocks.

1.5 Expected scientific impact

The full knowledge of shock micro-processes will more firmly establish our knowledge of fundamental plasma processes. This will further enable collaboration with the laboratory plasma community, as they develop and experiment with similar scale and mechanisms. This will also enable greater collaboration with the astrophysical community, as they observe astrophysical shocks via remote sensing. The observed radiation from these shocks stem from the post-energy conversion process. By acquiring an accurate knowledge of energy partitioning resulting from collisionless shocks, we will establish clearer connections to the processes and implications in shocks beyond our *in-situ* capabilities.

2 Why this science cannot be done with MMS and cluster

MMS is the most sophisticated technology we currently have to measure space plasma *in-situ*. It can measure full electron velocity distributions over a 30 m cadence and partial distributions as low as 7.5 m. It is the most capable mission we have to observe microscale phenomena in the bow shock. And indeed it has, and opened up a completely new avenue into the discussion of the physics that take place in collisionless shocks. However, MMS cannot provide scientific closure to the stated questions concerning collisionless shocks. In this section, we outline the most critical reasons behind this statement.

Firstly and most critically, MMS cannot resolve the ion solar wind beam distribution. Due to its design, MMS particle detectors (both FPI and HPCA) are not optimized to resolve the proton energy distribution of the solar wind. Figure 5 shows the MMS energy coverage of modeled solar wind populations in comparison to Wind. The proton core population is insufficiently resolved to determine even basic moments such as density and temperature. Nor can the strahl electron population above ~500 eV be captured as count rates fall below statistical significance. Without accurate resolution of these populations, we cannot characterize the upstream plasma nor observe the solar wind development through the shock (Wilson et al., 2022).

Secondly, the electric field probes are too long to accurately measure high frequency wave phenomena (see Figure 3). Observed short wavelength waves appear highly attenuated from the very long boom lengths, rendering them very difficult to analyze. We can resolve this through careful interferometry and application of theory. However, assumptions will always be made to do so and we therefore cannot make significant progress to understanding the

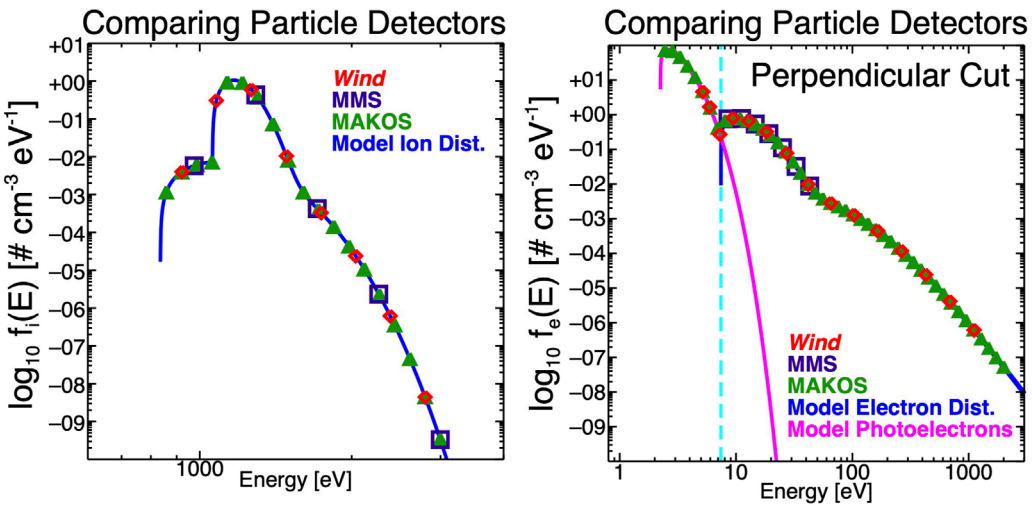

FIGURE 5
Comparison of Wind, MMS, and MAKOS proton (left) and electron (right) energy resolution overlaid on model solar wind VDFs. Note MMS's inability to resolve the solar wind proton peak, and the lack of statistically significant electron counts above ~500 eV.

roles waves take in energy conversion within the terrestrial bow shock.

Finally, the MMS spacecraft separation distances do not allow for appropriate simultaneous upstream and downstream measurements. MMS has had an average of ~15 km separation in the dayside magnetosphere, well within the solar wind gyroradius (~1,000 km). This is not sufficient distance to determine the conditions of unperturbed solar wind. These scales can be adjusted to enable cross-scale measurements within the realm of the bow shock and magnetosheath. However, even if appropriate distances can be achieved, the two previous outstanding issues remain.

To summarize, MMS is insufficient to deliver accurately on MAKOS science objectives for the following reasons:

1. Insufficient particle instrument performance in the solar wind;
2. Limiting/restrictive assumptions concerning short wavelength E-field data inherent to the instrument design; and
3. Inadequate inter-spacecraft separations and orbital configuration.

Cluster is also insufficient to deliver accurately on MAKOS science objectives for the following reasons:

1. Insufficient particle instrument performance in the solar wind (similar to Wind energy resolution shown in Figure 5);
2. Insufficient temporal resolution; and
3. Sufficient spacing at ion kinetic scales but insufficient spacing at MHD scales.

The MAKOS mission and observatories are explicitly designed to provide the required multipoint spatial distribution, high temporal resolution, and energy and angular resolution (particles, particularly in the solar wind) to fully quantify the energy budget and characterize the dominant energy conversion mechanisms at collisionless shocks for the first time.

3 Investigation Description

3.1 Mission overview

The baseline MAKOS mission concept comprises four spacecraft (S/C) with varying spatial separations at ion-kinetic to MHD scales in high-altitude, slightly elliptical (23.1 × 18.0 R_E) five-to-one (5:1) lunar resonance orbits (LROs) with oppositely oriented lines of apsides that maximize the number of bow shock crossings, even when apogee is on the nightside. Each of the two orbits has two S/C with separations on the order of ~100—1,000 km to obtain the required simultaneous upstream, downstream, and transition layer observations at shocks, including multipoint observations at ion-kinetic scales through every shock transition layer crossing. The separations between the S/C on the different orbits range from ~5 to 12 R_E. This provides year-round crossings of the bow shock with simultaneous multipoint separations ranging from ion kinetic (100—1,000 km; each pair) to MHD (several R_E; the pair of pairs) scales, as well as prolong ed dwell time throughout the year in the solar wind, enabling opportunities to also study interplanetary (IP) shocks and for MAKOS to simultaneously probe electron- and ion-kinetic plus MHD-scale processes during every single bow shock and IP shock crossing (>1,000 expected during MAKOS' 2-year prime mission).

MAKOS requires each S/C to carry a comprehensive science payload of particles, fields, and waves instruments specifically tailored to measure the *in-situ* processes at play in collisionless shocks. The need to resolve microphysical phenomena in and around each shock and to fully characterize the plasma populations upstream and downstream of each shock drives a mission requirement that the complete three-dimensional thermal and suprathermal electron and ion velocity distributions be sampled at very high temporal resolution (<1 s). This is achieved in the notional mission design by carrying multiple dedicated sensors targeting each

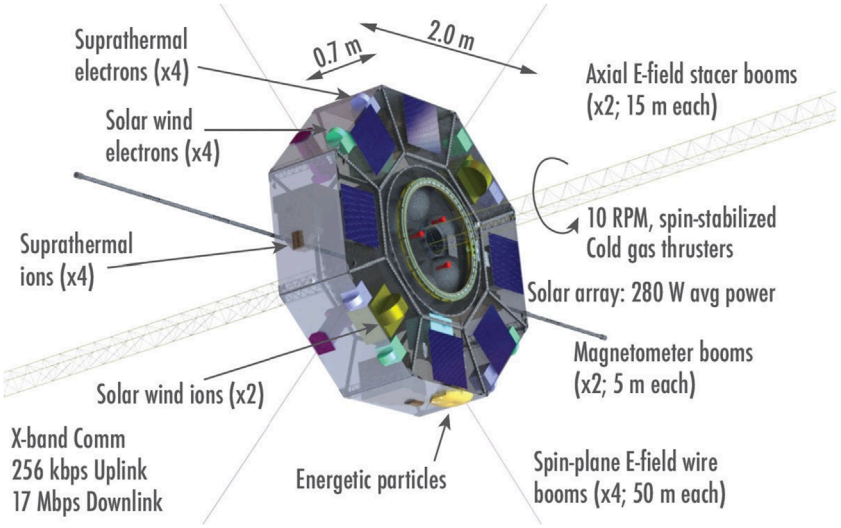

FIGURE 6
An illustrated schematic of a single MAKOS spacecraft with its full instrument suite.

TABLE 1 MAKOS carries a high-TRL (≥6) payload specifically tailored to measure the electromagnetic fields and particle populations required to understand energy partitioning and conversion processes at collisionless shocks. Particle detectors are shaded in gray. Fields instruments are shaded in white.

Instrument	#	CBE per unit (kg)	CBE total (kg)	CBE per unit (W)	CBE total (W)
SWI	2	3.5	7.0	3.5	7.0
SWE	4	2.6	10.4	3.2	12.8
STI	4	11.4	45.6	12.0	48.0
STE	4	2.6	10.4	3.2	12.8
EP	1	3.9	3.9	3.8	3.8
FGM	2	0.7	1.4	4.0	8.0
SCM	1	0.8	0.8	1.0	1.0
EF	1	22.0	22.0	8.4	8.4
Totals			101.5		101.8

species and energy range on a rapidly-spinning (10 RPM baseline) S/C. Furthermore, the need to resolve the evolution of the solar wind ion beam necessitates a dedicated detector, that is, constantly pointed into the solar wind - i.e., along a S/C spin vector anti-aligned with the solar wind flow direction.

3.2 Science payload

The MAKOS science payload will consist of a full particle and fields instrument suite totalling eight detectors. These instruments are illustrated on one of the MAKOS spacecraft in Figure 6. The resource demands of the MAKOS science payload are summarized in Table 1 and instrument details are listed below.

3.2.1 Solar Wind Ions (SWI)

Two SWI sensor heads—based on the PSP/SWEAP/SPAN-I instrument (Kasper et al., 2016; Whittlesey et al., 2020)—will be oriented such that their fan-like, planar (40°× ~6°) fields-of-view (FOVs) are orthogonal to each other and both parallel to the nominal solar wind direction, i.e., roughly parallel to the S/C spin axis.

3.2.2 Solar Wind Electrons (SWE)

Four SWE detector heads—based on the WIND/3DP/EESA-L sensor (Lin et al., 1995)—will each view the sky with a fan-like >180 °× 3° FOV (coplanar with S/C spin axis) pointing outward at ~90° spacing around the S/C.

3.2.3 Suprathermal Ions (STI)

Four STI detector heads—based on the STEREO/PLASTIC instrument (Galvin et al., 2008)—will each view the sky with a fan-like ~180°× 6° FOV (coplanar with the S/C spin axis) pointing radially outward at ~90° spacing around the S/C to achieve the 4π-sr sky coverage and temporal resolution required for MAKOS.

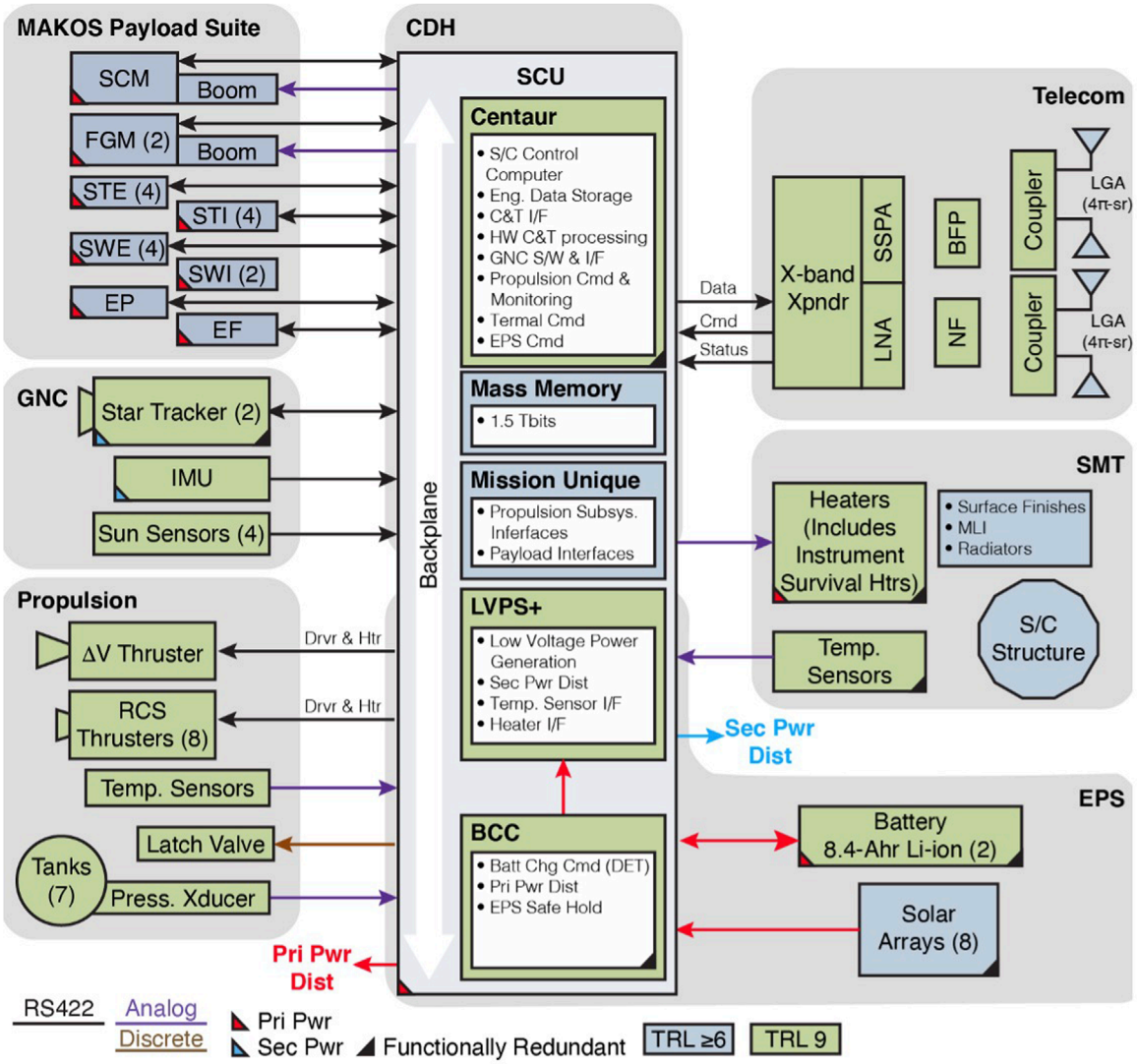

FIGURE 7
The MAKOS observatory reference design uses a single-string architecture with functional redundancy with heritage from the NASA CYGNSS mission.

3.2.4 Suprathermal Electrons (STE)

Four STE detector heads—based on the Wind/3DP/EESA-H instrument (Lin et al., 1995)—will each view the sky with a fan-like ~180°× 14° FOV (coplanar with the S/C spin axis)—i.e., only half the EESA-H azimuthal range - pointing radially outward at ~90° spacing around the S/C to achieve the 4π-sr sky coverage and temporal resolution required for MAKOS.

3.2.5 Energetic Particles (EP)

Each MAKOS S/C will carry a single EP sensor based on the time-of-flight-by-total energy PSP/ISΘIS/EPI-Lo instrument (McComas et al., 2016; Hill et al., 2017)—with a nearly 2π-sr FOV.

3.2.6 Fluxgate Magnetometer (FGM)

Two FGM sensors—based on the MMS/FIELDS/FGM tri-axial (orthogonal to within ~1°), fluxgate instrument (Russell et al., 2014; Torbert et al., 2016)—will be mounted on a common 5-m, single-hinged boom in a "gradiometer" configuration to characterize and eliminate S/C signals of electromagnetic interference. It is assumed that the main MAKOS/FGM electronics will be housed in a common "fields" electronics box housing along with those of the SCM and EF instruments.

3.2.7 Search Coil Magnetometer (SCM)

The three-axis SCM sensor—based on three orthogonal (to within ~1°) instances of the search coil magnetometer of the Juno/WAVES instrument (Kurth et al., 2017)—will be mounted on a second 5-m, single-hinged boom (identical but oppositely mounted from the FGM boom). The MAKOS/SCM electronics will also be housed in the common "fields" electronics box.

3.2.8 Electric Fields (EF)

The three-axis EF instrument—based on the MMS/FIELDS/ADP (axial) and SPD (spin-plane) instruments (Ergun et al., 2016; Lindqvist et al., 2016; Torbert et al., 2016)—will comprise twelve spherical voltage probes mounted on four 50-m wire booms in the

TABLE 2 The MAKOS S/C performance is more than sufficient to meet the mission's science requirements and instrument accommodations. Rows are shaded to differentiate categories.

Parameter/Item		Performance	Parameter/Item		Performance
Structure	Type	CFRP panels with milled Al supports	Space to Ground Communications	Uplink	X-band 256 kbps
	Size	Octagonal; 2.0 m × 0.65 m		Data Downlink	Science: 17 Mbps Engineering: 256 kbps
	1st Mode	>210 Hz			
	SV Mass (dry)	315.7 kg	Data	Data Storage	1,312 GBytes
Thermal	Architecture	Cold bias	Attitude Knowledge	Star Tracker	Dual, 20 arc-sec (1σ)
	Control	Heaters, MLI, radiators		IMU	Bias Stability: 0.3°/hr
Solar Array	Configuration	6-panel, body mounted	Attitude Control	Performance	<30 arc-sec (1σ)
	Size	0.84m^2		Architecture	Spin stabilized, 10 rpm
	Cell Type	Triple junction with AR coating		Pointing	<1.3 deg
	Cell Efficiency	28.4% (EOL)		Nutation	<1.6 deg (p-p)
	Full power output	283 W (EOL)	Orbital Knowledge	GPS position	<100 m (1σ)
Battery	Configuration	8 cells/10 strings (8p10s) (x2)		Velocity	<10 cm/s (1σ)
	Cell type	Li-ion	Propulsion	Type	Cold Gas (SF6)
	Capacity	56 Ahr		DeltaV Thrusters	1N, Isp: 45 s (qty 3)
	DOD during full eclipse periods	<49% with no operational restrictions		RCS Thrusters	120mN, Isp: 45 s (qty 8)
Power	Average Load	149.5 W (cold case)		Delta-V	>160 m/s when fully loaded
	Margin	90%		Reaction Control	6 degrees of freedom

spin-plane of the S/C and two 10-m stacer booms along its spin-axis (i.e., axial). EF will employ two probes [as implemented on the FAST mission (Ergun et al., 2001)]—separated by 10 m - on each boom to accurately resolve wave phenomena with wavelengths 100 m.

3.3 MAKOS spacecraft reference design

The MAKOS observatories comprise the MAKOS payload integrated with a spin-stabilized S/C using a single-string hardware architecture with functional and selective redundancy included for critical areas. The architectural approach achieves a mission success of >90% over its two-year mission lifetime as demonstrated by the NASA CYGNSS eight-observatory mission (Rose et al., 2013), which has operated for over 5 years without failure.

The simple operational nature of the MAKOS instruments and science profile allows significant autonomous on-board control of the observatory during all normal science and communication operations without need for daily on-board command sequences. Observatory initialization and science operations use five sub-modes: rate damping, nutation damping, Sun acquisition/precession control, spin-rate control, and science. After initial damping of launch vehicle separation rates is complete, the observatory transitions to Sun acquisition using Sun sensors and a sky-searching algorithm to locate the Sun vector. The observatory then uses reaction control thrusters to point the S/C solar arrays at the Sun using the rate and Sun sensors. The star trackers are initialized followed by spin-up of the S/C to its operational spin rate of 10 rpm. The vehicle spin axis then precesses to align with the local solar wind vector for science operations.

The MAKOS observatory design (Figure 7 and Table 2) is mission-specific to meet science requirements and instrument accommodations. Physical accommodation of the MAKOS instruments and spin stabilization implementation drives the observatory's structure and thermal design. Fixed solar arrays, located on the Sun-oriented face of the observatory provide electrical power for the S/C. The LRO enables use of a simple direct energy transfer architecture for battery charging with the batteries sized to accommodate full science operations during solar eclipse periods. Primary attitude knowledge is star tracker-based augmented with rate sensors for stability and nutation determination.

Sun sensors are included for emergency operations. Observatory orientation, spin-rate and precession are all controlled using an on-board cold-gas SF6-based reaction control subsystem. Observatory positional knowledge is based on GPS receivers augmented by on-board optical navigation during GPS outages. Communication is provided by an X-band transponder and low-gain patch antennas to provide communications without interrupting science operations. On-board timing requirements are driven by science data synchronization within the constellation relative to measurement of the solar wind and electric field waveforms. Specific S/C performance characteristics are provided in Figure 2 and Table 2. Observatory magnetic and electrostatic cleanliness is key to the MAKOS instruments meeting science

Level 1 requirements. MAKOS uses mature electromagnetic requirements consistent with previous missions (e.g., MMS, Cluster, THEMIS) to develop a magnetically and electrostatically clean observatory.

Expected science data generated is 53.5 GB/orbit. Baseline on-board data storage provides 188 GB or 3.5 orbits of science data storage to allow for recovery from downlink anomalies. The baseline reference communication uses a 14 Mbps X-band RF link that, with 14% overhead for CCSDS, requires ~9.6 h to downlink science data from 1 orbit. Significantly improved data rates would be available to reduce downlink durations and/or increase data downlink quantities if the optical communications are realized prior to MAKOS implementation.

3.4 Concept of operations

Telemetry is a major driver of the notional MAKOS mission design as the science requires very high data rates for observatory science telemetry at and around each collisionless shock crossing. Furthermore, MAKOS should also capture the highest rate data from any interplanetary shocks encountered upstream of the bow shock. Despite this, the MAKOS concept of operations (CONOPS) (Figure 8) is simple by design and consists of collecting science data (telemetry) from each of the four identical observatories during the two-year prime science mission. Each observatory will record telemetry in one of two science modes: 1) high-rate and 2) low-rate. Even under extreme solar wind driving conditions, the bow shock is consistently located outside of the average (i.e., typical) magnetopause location. Thus, the average magnetopause location offers an opportune surface to use for routine orbit-to-orbit operations and systematically toggling the MAKOS S/C between high- (i.e., along the orbit beyond the average magnetopause location) and low-rate (i.e., along the orbit within the average magnetopause location) modes. Using the average magnetopause location and the orbit predicts to schedule onboard science telemetry mode changes, each MAKOS observatory shall switch from low-to high-rate data collection when it transits from the magnetopause into the magnetosheath (i.e., outbound model magnetopause crossings), and each observatory will switch from high-to low-rate data collection when it transits from the magnetosheath into the magnetosphere (i.e., inbound magnetopause crossings).

The MAKOS payload generates data at either 807 kbps (low-rate) or 20.875 Mbps (high-rate) to achieve the temporal resolutions required for each observable. Acquiring high-rate data only when the S/C are sunward of the average magnetopause requires high-rate telemetry being recorded for ~60 h (46%) of each 5.46-day orbit.

However, all 611 GB of science data per orbit cannot be transmitted to ground each orbit because of limitations of the communications subsystem and ground network. To ensure that all collisionless shock transits are captured during the prime mission, MAKOS will employ a "scientist-in-the-loop" (SITL) strategy similar to that used by MMS (Fuselier et al., 2016). A trained MAKOS science and data expert (i.e., SITL) will review a special low-rate data product produced onboard and telemetered to ground each orbit to make prioritized selections of which periods of the high- and low-rate data shall be telemetered to the ground. Shock crossings will be prioritized, and data from and around each shock crossing will be telemetered to the ground to ensure prime science closure. The expected SITL-selected high-rate data volume averages 5.9 GB (~1% of recorded data) per S/C per orbit; combined with the low-rate data generated each orbit (47.6 GB per S/C), this yields 53.5 GB of data to be telemetered to ground from each MAKOS S/C each orbit (9% of 595 GB total recorded data). Over the two-year prime mission, all four MAKOS S/C will telemeter 28.6 TB of total 327 TB scientific data recorded.

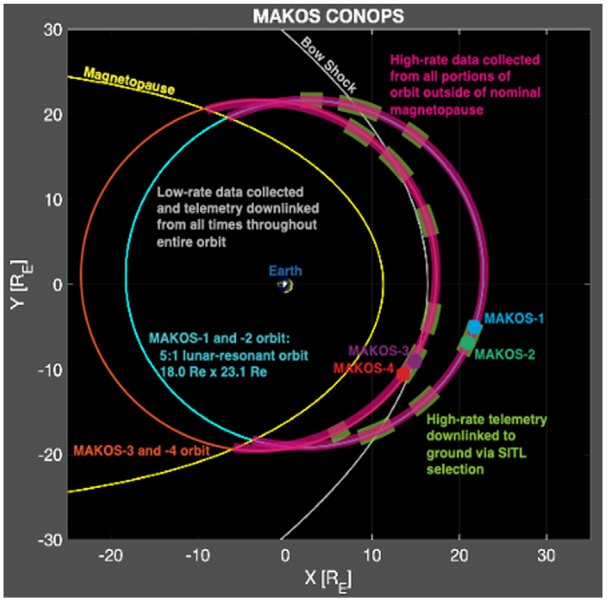

FIGURE 8
MAKOS uses two identical, 180°-phased LROs to achieve its target inter-S/C separations. A proven SITL process will be used to prioritize high-rate data obtained during predefined portions of the orbit for downlink.

3.5 Mission cost, risk, and schedule

The four-observatory configuration will require $651M (FY22) funding as a current best estimate. Recognizing that this is a preliminary concept study, conservative reserves are applied to all cost elements: 50% for all Phase B-D work and 25% for Phase E-F. This brings the baseline estimate to $964M (with NASA's addition of a Phase A study and Launch Services to complete the funding). Additional development costs are not included, as baseline instruments and supporting hardware were chosen to be at TRL 6 prior to Phase A.

The MAKOS risk assessment combined with cost to identify key risks is likely to drive significant variances if not managed. A four-observatory constellation, each carrying eight instruments, is within the overall experience base of the institutional partners, but the need to deliver multiple flight units raises the criticality of certain common development issues. Figure 9 shows the top-level schedule with major milestones. Table 3 lists the top three identified risks and potential mitigations.

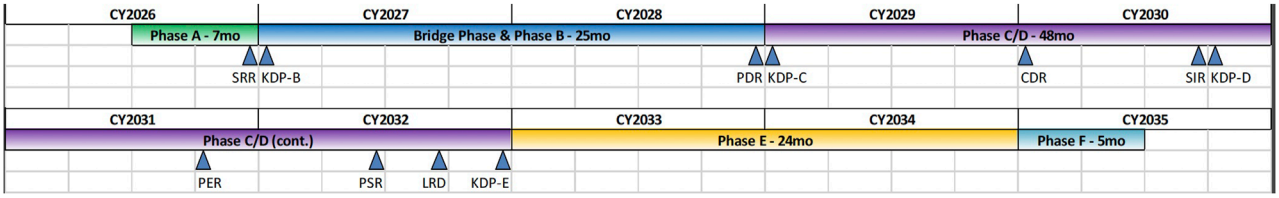

FIGURE 9
The MAKOS development plan baselines 79 months for Phases A–D, with a staggered observatory AI&T approach - including a 3-month cruise and commissioning, followed by a 2-year Phase E.

TABLE 3 MAKOS has no severe mission risks and favorable mitigations for the top three identified risks. (L = risk likelihood, C = risk consequence).

#	Risk	Type	L	C	Mitigation
1	IF a launch issue precludes all four S/C from achieving the necessary formation, THEN there could be delay to the science phase and/or impact to science closure	Cost, Schedule	1	5	Phase A trades will consider additional propulsion capacity in S/C design to potentially enable achievement of baseline MAKOS configuration from a single launch
2	IF instrument cross-calibration requires more analysis to resolve known challenges and ensure data product adequacy, THEN additional effort would be required	Cost, Technical	3	2	Use of advanced data analytic techniques to develop novel ways to cross-correlate the data using timing, position, and events to improve completeness of datasets for science would be required
3	IF specialized component updates are needed for the EF instrument deployment mechanism, THEN additional development effort would be required	Cost, Technical	2	2	Additional design, prototyping, and testing will be conducted to reduce likelihood of failure of the EF deployment mechanism

3.6 Enhancing technology development needs

3.6.1 Instrument Development

Obtaining more comprehensive 3D particle measurements at cadences even faster (e.g., 10-m) than recent missions (e.g., MMS and Parker Solar Probe)—without relying on a high number of sensors—will require additional instrument development for traditional top-hat ESAs or development of new particle detection systems for low-energy space plasmas. Particular emphasis is needed in two key areas: 1) parts availability, e.g., reliable high voltage optocouplers, and 2) tuning and responsiveness of the high voltage power supplies to ensure fast measurements are being taken with sufficient accuracy. At least one vendor that has provided flight parts for previous NASA missions has existing custom optocoupler designs that can fulfill even the most ambitious high-resolution MAKOS measurement cadences.

3.6.2 Infrastructure

While MAKOS achieves its baseline science with current RF communications infrastructure, it requires limiting high-rate data collection to only targeted portions of the orbit. Even downlinking data only when S/C are earthward of the magnetopause (i.e., ~71-h/orbit window) requires hours per day per S/C of DSN time. Optical communications would drastically reduce required downlink, thus enabling significantly more science data to be downlinked and reducing SITL decisions and complexity. The much higher data rates afforded by optical downlink would enhance MAKOS by significantly reducing resource competition and/or providing additional science data and reducing the need for SITL-based operations.

4 Summary and conclusion

In all applications of space plasmas, three universal plasma processes dominate the dynamics. Magnetic reconnection reconfigures topologies, allows plasma mixing and can drive flows and acceleration. Turbulence transfers energy to small scales where it can be efficiently dissipated.x.

Collisionless shocks are a fundamental plasma process. They are the prime “thermalizers” (converting flow energy to heat) and “non-thermalizers” (converting flow energy to nonthermal features and energetic particles) in the astrophysical world. Despite that importance, and decades of observations and thoeretical/simulational studies, the basic ability to predict how a shock with given upstream parameters will partition the incident energy amongst the various degrees of freedom available remains elusive. This white paper has laid out the questions that need to be answered to address this ignorance, the reasons why existing missions and datasets cannot provide a complete answer, and the capabilities a dedicated mission must have in order to do so.

The heliophysics community recognizes the importance of fundamental processes through the support of the previously launched Magnetospheric Multiscale (MMS) mission and the recently selected Mid-Explorer Helioswarm mission. Both were selected with the intent of observing magnetic reconnection and plasma turbulence respectively. In order to achieve a complete view of the fundamental physics that dominate our Universe,

collisionless shocks must also be considered a subject of importance in heliophysics. This can and must be done by supporting targeted opportunities to observe the terrestrial bow shock *in-situ*, starting with MAKOS.

Data availability statement

The original contributions presented in the study are included in the article/Supplementary Material, further inquiries can be directed to the corresponding author.

Author contributions

All authors listed have made a substantial, direct, and intellectual contribution to the work and approved it for publication.

Funding

The output of this concept study was made possible by the NASA Heliophysics Mission Concept Study (HMCS) award (80NSSC22K0111).

Acknowledgments

Some of the work was supported by the Geospace Environment Modeling Focus Group "Particle Heating and Thermalization in Collisionless Shocks in the Magnetospheric multiscale mission (MMS) Era" led by LW.

Conflict of interest

The authors declare that the research was conducted in the absence of any commercial or financial relationships that could be construed as a potential conflict of interest.

Publisher's note

References

Bale, S. D., and Mozer, F. S. (2007). Measurement of large parallel and perpendicular electric fields on electron spatial scales in the terrestrial bow shock. *Phys. Rev. Lett.* 98, 205001. doi:10.1103/PhysRevLett.98.205001

Breneman, A. W., Cattell, C. A., Kersten, K., Paradise, A., Schreiner, S., Kellogg, P. J., et al. (2013). STEREO and wind observations of intense cyclotron harmonic waves at the earth's bow shock and inside the magnetosheath: BOW SHOCK cyclotron harmonic waves. *J. Geophys. Res.* 118, 7654–7664. doi:10.1002/2013JA019372

Burgess, D. (2015). *Collisionless shocks in space plasmas*. Cambridge University Press.

Chen, L.-J., Wang, S., Wilson, L., Schwartz, S., Bessho, N., Moore, T., et al. (2018). Electron bulk acceleration and thermalization at earth's quasiperpendicular bow shock. *Phys. Rev. Lett.* 120, 225101. doi:10.1103/PhysRevLett.120.225101

Ergun, R. E., Carlson, C., Mozer, F., Delory, G., Temerin, M., McFadden, J., et al. (2001). *Space Sci. Rev.* 98, 67–91. doi:10.1023/A:1013131708323

Ergun, R., Tucker, S., Westfall, J., Goodrich, K. A., Malaspina, D. M., Summers, D., et al. (2016). The axial double probe and fields signal processing for the MMS mission. *Space Sci. Rev.* 199, 167–188. doi:10.1007/s11214-014-0115-x

European Commission (2021). *The foreshock and its role in solar-terrestrial relations*. Available at: https://cordis.europa.eu/project/id/704681/reporting.

Fuselier, S. A., Lewis, W. S., Schiff, C., Ergun, R., Burch, J. L., Petrinec, S. M., et al. (2016). Magnetospheric multiscale science mission profile and operations. *Space Sci. Rev.* 199, 77–103. doi:10.1007/s11214-014-0087-x

Galvin, A. B., Kistler, L. M., Popecki, M. A., Farrugia, C. J., Simunac, K. D. C., Ellis, L., et al. (2008). The plasma and suprathermal ion composition (PLASTIC) investigation on the STEREO observatories. *Space Sci. Rev.* 136, 437–486. doi:10.1007/s11214-007-9296-x

Gingell, I., Schwartz, S. J., Burgess, D., Johlander, A., Russell, C. T., Burch, J. L., et al. (2017). MMS observations and hybrid simulations of surface ripples at a marginally quasi-parallel shock. *J. Geophys. Res.* 122. doi:10.1002/2017JA024538

Goodrich, K. A., Ergun, R., Schwartz, S. J., Wilson, L. B., Johlander, A., Newman, D., et al. (2019). Impulsively reflected ions: A plausible mechanism for ion acoustic wave growth in collisionless shocks. *J. Geophys. Res.* 124, 1855. doi:10.1029/2018JA026436

Goodrich, K. A., Ergun, R., Schwartz, S. J., Wilson, L. B., Newman, D., Wilder, F. D., et al. (2018). MMS observations of electrostatic waves in an oblique shock crossing. *J. Geophys. Res.* 123, 9430–9442. doi:10.1029/2018JA025830

Hill, M. E., Mitchell, D. G., Andrews, G. B., Cooper, S. A., Gurnee, R. S., Hayes, J. R., et al. (2017). The mushroom: A half-sky energetic ion and electron detector. *J. Geophys. Res. Space Phys.* 122, 1513–1530. doi:10.1002/2016JA022614

Kasper, J. C., Abiad, R., Austin, G., Balat-Pichelin, M., Bale, S. D., Belcher, J. W., et al. (2016). Solar wind electrons alphas and protons (SWEAP) investigation: design of the solar wind and coronal plasma instrument suite for solar probe plus. *Space Sci. Rev.* 204, 131–186. doi:10.1007/s11214-015-0206-3

Kurth, W. S., Hospodarsky, G. B., Kirchner, D. L., Mokrzycki, B. T., Averkamp, T. F., Robison, W. T., et al. (2017). The Juno waves investigation. *Space Sci. Rev.* 213, 347–392. doi:10.1007/s11214-017-0396-y

Lin, R., Anderson, K. A., Ashford, S., Carlson, C., Curtis, D., Ergun, R., et al. (1995). A three-dimensional plasma and energetic particle investigation for the wind spacecraft. *Space Sci. Rev.* 71, 125–153. doi:10.1007/BF00751328

Lindqvist, P.-A., Olsson, G., Torbert, R. B., King, B., Granoff, M., Rau, D., et al. (2016). The spin-plane double probe electric field instrument for MMS. *Space Sci. Rev.* 199, 137–165. doi:10.1007/s11214-014-0116-9

McComas, D. J., Alexander, N., Angold, N., Bale, S., Beebe, C., Birdwell, B., et al. (2016). Integrated science investigation of the Sun (ISIS): design of the energetic particle investigation. *Space Sci. Rev.* 204, 187–256. doi:10.1007/s11214-014-0059-1

Rose, R., Ruf, C., Rose, D., Brummitt, M., and Ridley, A. (2013). The CYGNSS flight segment; A major NASA science mission enabled by micro-satellite technology. *IEEE Aerosp. Conf. Proc.* doi:10.1109/AERO.2013.6497205

Russell, C., Anderson, B. J., Baumjohann, W., Bromund, K. R., Dearborn, D., Fischer, D., et al. (2014). The magnetospheric multiscale magnetometers. *Space Sci. Rev.* 199, 189–256. doi:10.1007/s11214-014-0057-3

Schwartz, S. J., Avanov, L., Turner, D., Zhang, H., Gingell, I., Eastwood, J. P., et al. (2018). Ion kinetics in a hot flow anomaly: MMS observations. *Geophys. Res. Lett.* 45, 511. doi:10.1029/2018GL080189

Schwartz, S. J., Goodrich, K. A., Wilson, L. B., Turner, D. L., Trattner, K. J., Kucharek, H., et al. (2022). Energy partition at collisionless supercritical quasi-perpendicular shocks. *J. Geophys. Res. Space Phys.* 127, e2022JA030637. doi:10.1029/2022JA030637

Torbert, R., Russell, C. T., Magnes, W., Ergun, R. E., Lindqvist, P. A., LeContel, O., et al. (2016). The FIELDS instrument suite on MMS: scientific objectives, measurements, and data products. *Space Sci. Rev.* 199, 105–135. doi:10.1007/s11214-014-0109-8

Tsurutani, B. T., and Rodriguez, P. (1981). Upstream waves and particles: an overview of ISEE results. *J. Geophys. Res.* 86, 4317–4324. doi:10.1029/JA086iA06p04317

Turner, D. L., Omidi, N., Sibeck, D. G., and Angelopoulos, V. (2013). First observations of foreshock bubbles upstream of Earth's bow shock: characteristics and comparisons to HFAs. *J. Geophys. Res.* 118, 1552–1570. doi:10.1002/jgra.50198

Vasko, I. Y., Mozer, F. S., Krasnoselskikh, V. V., Artemyev, A. V., Agapitov, O. V., Bale, S. D., et al. (2018). Solitary waves across supercritical quasi-perpendicular shocks. *Geophys. Res. Lett.* 45, 5809–5817. doi:10.1029/2018GL077835

Wang, S., Chen, L., Hesse, M., Gershman, D. J., Dorelli, J., Giles, B., et al. (2016). Ion demagnetization in the magnetopause current layer observed by MMS. *Geophys. Res. Lett.* 43, 4850–4857. doi:10.1002/2016GL069406

Whittlesey, P. L., Larson, D. E., Kasper, J. C., Halekas, J., Abatcha, M., Abiad, R., et al. (2020). The solar probe ANalyzers—electrons on the parker solar probe. *Astrophysical J. Suppl. Ser.* 246, 74. doi:10.3847/1538-4365/ab7370

Wilson, L. B., III, Koval, A., Sibeck, D. G., Szabo, A., Cattell, C. A., Kasper, J. C., et al. (2013). Shocklets, SLAMS, and field-aligned ion beams in the terrestrial foreshock. *J. Geophys. Res.* 118, 957–966. doi:10.1029/2012JA018186

Wilson, L. B., Sibeck, D. G., Breneman, A. W., Contel, O. L., Cully, C., Turner, D. L., et al. (2014a). Quantified energy dissipation rates in the terrestrial bow shock: 1. Waves and dissipation. *J. Geophys. Res.* 119, 6455. doi:10.1002/2014JA019929

Wilson, L. B., Sibeck, D. G., Breneman, A. W., Contel, O. L., Cully, C., Turner, D. L., et al. (2014b). Quantified energy dissipation rates in the terrestrial bow shock: 2. Analysis techniques and methodology. *J. Geophys. Res.* 119, 6475. doi:10.1002/2014JA019930

Wilson, L. B., Sibeck, D., Turner, D., Osmane, A., Caprioli, D., and Angelopoulos, V. (2016). Relativistic electrons produced by foreshock disturbances observed upstream of earth's bow shock. *Phys. Rev. Lett.* 117, 215101. doi:10.1103/PhysRevLett.117.215101

Wilson III, L. B., Goodrich, K. A., Turner, D. L., Cohen, I. J., Whittlesey, P. L., and Schwartz, S. J. (2022). The need for accurate measurements of thermal velocity distribution functions in the solar wind. *Front. Astronomy Space Sci.* 9, 1063841. doi:10.3389/fspas.2022.1063841